HUMAN GENE THERAPY 23:1101–1115 (October 2012)

DOI: 10.1089/hum.2012.125

The Human Rhodopsin Kinase Promoter in an AAV5 Vector Confers Rod- and Cone-Specific Expression in the Primate Retina

Shannon E. Boye,[1,*] John J. Alexander,[2,*] Sanford L. Boye,[1] Clark D. Witherspoon,[2] Kristen J. Sandefer,[2] Thomas J. Conlon,[3] Kirsten Erger,[3] Jingfen Sun,[1] Renee Ryals,[1] Vince A. Chiodo,[1] Mark E. Clark,[4] Christopher A. Girkin,[4] William W. Hauswirth,[1] and Paul D. Gamlin[2]

Abstract

Adeno-associated virus (AAV) has proven an effective gene delivery vehicle for the treatment of retinal disease. Ongoing clinical trials using a serotype 2 AAV vector to express *RPE65* in the retinal pigment epithelium have proven safe and effective. While many proof-of-concept studies in animal models of retinal disease have suggested that gene transfer to the neural retina will also be effective, a photoreceptor-targeting AAV vector has yet to be used in the clinic, principally because a vector that efficiently but exclusively targets all primate photoreceptors has yet to be demonstrated. Here, we evaluate a serotype 5 AAV vector containing the human rhodopsin kinase (hGRK1) promoter for its ability to target transgene expression to rod and cone photoreceptors when delivered subretinally in a nonhuman primate (NHP). *In vivo* fluorescent fundus imaging confirmed that AAV5-hGRK1-mediated green fluorescent protein (GFP) expression was restricted to the injection blebs of treated eyes. Optical coherence tomography (OCT) revealed a lack of gross pathology after injection. Neutralizing antibodies against AAV5 were undetectable in post-injection serum samples from subjects receiving uncomplicated subretinal injections (i.e., no hemorrhage). Immunohistochemistry of retinal sections confirmed hGRK1 was active in, and specific for, both rods and cones of NHP retina. Biodistribution studies revealed minimal spread of vector genomes to peripheral tissues. These results suggest that AAV5-hGRK1 is a safe and effective AAV serotype/promoter combination for targeting therapeutic transgene expression protein to rods and cones in a clinical setting.

Introduction

Recombinant adeno-associated virus (AAV) has emerged as the optimal gene delivery vehicle to treat retinal diseases requiring expression of a specific protein. AAV is attractive because of its safety, long-term expression, ability to transduce terminally differentiated cells, and broad yet selective tropism through the use of the numerous AAV serotypes currently available (Daya and Berns, 2008; Vandenberghe and Auricchio, 2012). It has been used successfully in proof of concept experiments in a variety of animal models of retinal disease (Stieger and Lorenz, 2010; Sundaram *et al.*, 2012). Ongoing clinical trials for *RPE65*-LCA (LCA2) highlight the ability of subretinally delivered AAV2 to express a therapeutic transgene in the retinal pigment epithelium, thereby restoring retinal function and visually evoked behavior to patients (Ashtari *et al.*, 2011; Bainbridge *et al.*, 2008; Bennett *et al.*, 2012; Cideciyan *et al.*, 2008; Hauswirth *et al.*, 2008; Jacobson *et al.*, 2012; Maguire *et al.*, 2008). However, because the majority of inherited retinal diseases are caused by defects in photoreceptor-specific genes (Dryja, 2001), the development of vectors that will safely and effectively target transgenes to this cell type is warranted.

Studies have shown that AAV5 exhibits increased tropism for photoreceptors and faster transduction kinetics relative to AAV2 (Auricchio *et al.*, 2001; Lotery *et al.*, 2003; Yang *et al.*, 2002). AAV5 has been shown to effectively target photoreceptors in mouse, dog, and nonhuman primate (NHP), and has been used successfully to restore retinal function and preserve retinal structure in models of various retinal

[1]Department of Ophthalmology and [3]Department of Pediatrics, University of Florida College of Medicine, Gainesville, FL 32610.
[2]Department of Vision Sciences and [4]Department of Ophthalmology, University of Alabama at Birmingham, Birmingham, AL 35294.
*These authors contributed equally to this work.

diseases, including retinoshisis, achromatopsia, LCA1, LCA2, and retinitis pigmentosa (Alexander *et al.*, 2007; Boye *et al.*, 2010; Gorbatyuk *et al.*, 2010; Komaromy *et al.*, 2010; Li *et al.*, 2011; Mancuso *et al.*, 2007; Mao *et al.*, 2011; Min *et al.*, 2005; Pang *et al.*, 2010; Pang *et al.*, 2008; Pang *et al.*, 2012a; Yao *et al.*, 2011). Recently, it has been shown that this serotype efficiently transduced cone photoreceptors and produced trichromatic color vision in an NHP model of red–green color blindness, making AAV5 the only serotype with demonstrated therapeutic efficacy in an NHP model of photoreceptor dysfunction (Mancuso *et al.*, 2009). While there is a strong impetus to develop AAV vectors that target cone photoreceptors due to their central role in high-acuity daylight vision, many diseases exist in which both rods and cones need to be targeted simultaneously, including, but not limited to, retinitis pigmentosa, cone-rod dystrophies, and Leber congenital amaurosis (LCA).

Several proof-of-concept studies have shown that, when used in conjunction with AAV, the human rhodopsin kinase (hGRK1) promoter efficiently drives therapeutic transgene expression exclusively in photoreceptors and restores retinal function to mouse models of human retinal disease (Beltran *et al.*, 2012; Boye *et al.*, 2010; Boye *et al.*, 2011; Khani *et al.*, 2007; Pawlyk *et al.*, 2010; Sun *et al.*, 2010; Tan *et al.*, 2009). It has been suggested that, due to its small size and proven activity in murine photoreceptors, hGRK1 is an optimal promoter choice for targeting rods and cones in a clinical setting. However, additional studies are needed for two reasons before reaching this conclusion. First, a recent study revealed that hGRK1 drives AAV-mediated transgene expression in rods, but not cones, of the canine retina (Beltran *et al.*, 2010). It was suggested that this was due to a species-specific difference in the expression of G-protein coupled receptor kinases in rods and cones. GRK1 is expressed in both rods and cones of the mouse and rat retina whereas, in dogs, its expression is limited to rods (Weiss *et al.*, 2001). In dogs, desensitization of cones is instead modulated by a cone-specific isoform, GRK7 (Weiss *et al.*, 2001). In the human and monkey retina, GRK1 is also expressed in both rods and cones, but in these species, it is coexpressed along with GRK7 in cones (Weiss *et al.*, 2001). The existence of multiple GRK isoforms in primate cones may, therefore, in theory, limit the ability of the hGRK1 promoter to efficiently target AAV-mediated transgene expression to these cells. Second, evidence that rodent models are relatively poor predictors of AAV transduction in primates continues to emerge (Ivanova *et al.*, 2010; Yin *et al.*, 2011). Moreover, the structural differences between primate and rodent retinas, most notably the existence of a cone-rich fovea in the former, warrants formal evaluation of AAV vector tropism in nonhuman primate (NHP) retina prior to clinical application.

Here, we evaluate the transduction profile of AAV5 containing the hGRK1 promoter-driving green fluorescent protein (GFP) following subretinal delivery in an NHP species (*Macaca nemestrina*). We compare these results to those found in mice injected subretinally with the identical vector. In addition, we evaluate the presence of neutralizing antibodies to AAV5 in pre- and post-injection serum samples, the spread of vector genomes outside the injection site in peripheral organs, and the existence of any off-target transgene expression in the retina and optic nerves of the NHP. Using *in vivo* imaging and post mortem histology, we also evaluate whether subretinal injection of this vector resulted in any gross pathology in NHP retina.

Methods

AAV vector

AAV vector plasmid containing the 292nt version of human rhodopsin kinase promoter (GRK1)–driving GFP was identical to that used previously (Beltran *et al.*, 2010). AAV vector plasmid was packaged in AAV serotype 5 and titered according to previously published methods (Jacobson *et al.*, 2006a; Zolotukhin, 2005). Upon titering of the bulk product, virus was diluted to 1×10^{12} vector genomes/ml in balanced salt solution (BSS) (Alcon, Fort Worth, TX) with 0.014 % Tween-20 (JT Baker, Philipsburg, NJ) and immediately aliquoted in appropriate volumes for NHP and mouse experiments, at 0.750 ml and 0.020 ml, respectively. Virus aliquots were stored at -80°C until shortly before injection.

Animals

All procedures performed on NHP and mice were approved by the Institutional Animal Care and Use Committee of the University of Alabama at Birmingham (UAB) and the University of Florida's Institutional Animal Care and Use Committee, respectively. All procedures were done in accordance with the Association for Research in Vision and Ophthalmology Statement for the use of animals in ophthalmic and vision research. Three male *Macaca nemestrina* (ages 6–7 yrs) and five, 5–6-week-old C57BL/6J mice (Jackson Laboratory, Bar Harbor, ME) were used in this study. NHP subject ET-79 was injected in October 2010. Subjects FK-34 and GD-59 were added to the study in October 2011.

Subretinal injection

All NHP surgical procedures were carried out under sterile conditions in a dedicated veterinary ophthalmic surgical suite. The subjects were sedated using 100 mg/ml Ketamine (10 mg/kg IM) and given subcutaneous 0.54 mg/ml atropine (0.05 mg/kg). An IV catheter was placed and a saline drip started, then the animal was intubated. Once sedated, the eyes were dilated using 2.5% phenylephrine/1% tropicamide/1% cylate. The animal was placed on a ventilator, and general anesthesia was carried out using Isoflurane (1.5% maintenance) while vital signs were continuously monitored. The right eye (subject ET-79) or left eye (subjects FK-34 and GD-59) were prepared with Betadine scrub and draped in standard sterile fashion. An Accurus 800CS surgical system with Xenon light source, Total Plus 23 gauge Vitrectomy Pak (Alcon, Inc., Fort Worth, TX) and Zeiss VISU 200 ophthalmic surgical microscope equipped with digital video (Endure Medical, Cumming, GA) were used for the surgery. The posterior segment retina was visualized using an irrigating Machemer magnifying vitrectomy contact lens (Ocular Instruments, Bellevue, WA). A standard 23-gauge three-port pars plana vitrectomy was performed with an inferior infusion cannula maintaining a continuous pressure of 30 mm/Hg with BSS Plus (Alcon, Inc., Fort Worth, TX). Subsequently, the superior-temporal sclerotomy was enlarged with a 20-gauge MVR blade for the injection cannula. A 39-gauge injection cannula with 20-gauge shaft (Synergetics, O'Fallon, MO) was used to

Table 1. Animal and Injection Details

ID #	*Age*[a]	*Injection date*	*Sacrifice*	*Eye inj.*	*Volume*	*Bleb location*	*Device*	*Vitrectomy*
ET-79	7 yrs	10/2/2010	48 days PI	R	60 μl 10^{12} VG/ml	Central plus superior	Synergetics	Standard
FK-34	7 yrs	8/13/2011	97 days PI	L	30 μl 10^{12} VG/ml	Central	Synergetics	Minimal
GD-59	6 yrs	8/13/2011	97 days PI	L	100 μl 10^{12} VG/ml 200 μl 10^{12} VG/ml	1. Peripheral-temporal 2. Central[b]	Lambert	Minimal

[a]All subjects were male.
[b]Possible reflux during injection.
PI, post-injection; R, right; L, left.

deliver vector into the subretinal space of subject ET-79's right eye through an injection located 2.5 mm superior-temporally to fovea in an area where no prominent vasculature was visualized. Approximately 60 microliters of AAV5-hGRK1-GFP containing 6×10^{10} vector genomes (vector concentration of 1×10^{12} particles/ml) was delivered creating a bleb in which a portion also extended under the fovea. This bleb measured approximately 5.0 mm in diameter (based on *in vivo* fluorescence fundus imaging). Injections for FK-34 and GD-59 were performed in a similar manner as described in Table 1. The three sclerotomy sites and conjunctiva were sutured closed using 9.0 vicryl, and subconjunctival cefazolin and dexamethasone were administered. To prevent corneal drying during surgical recovery, triple antibiotic ophthalmic ointment was applied to both eyes. Upon full recovery, the subject received intramuscular 0.3 mg/ml buprenex (0.01 mg/kg) BID for 3 days and 330 mg/ml cefazolin (25 mg/kg) BID for 7 days. Recovery was uneventful; the corneas of the treated eyes remained clear with only mild conjunctival redness, which resolved within a week after surgery.

The same AAV5-hGRK1-GFP virus prep was also used in our mouse experiments. A total of one microliter containing 1×10^{9} vector genomes (vector concentration 1×10^{12} particles/ml) was delivered to the subretinal space of five postnatal day 40 (P40) C57BL/6J mice (one eye only). Subretinal injections were performed according to methods previously described (Timmers *et al.*, 2001).

In vivo *imaging*

Imaging of ET-79 was performed at 3 weeks and 5 weeks post-injection (the right eye was examined for any baseline autofluorescence 5 days prior to surgery). Imaging of FK-34 and GD-59 was performed at 2.5 weeks and 5 weeks post-injection. Subjects were sedated using Ketamine/Acepromazine (10 mg/kg and 0.55 mg/kg, respectively) then the eyes were dilated using 2.5% phenylephrine/1% tropicamide. For corneal lubrication, Refresh (Allergan, Irvine, CA) or BSS drops were used. Once fully dilated, the subjects were situated on a custom table, in the "sphinx" position for imaging, using a Spectralis HRA+OCT (Heidelberg Engineering, Inc., Germany) scanning laser ophthalmoscope. Images were obtained with the 30-degree objective using infrared (820 nm) and autofluorescence (488 nm) modes with and without optical coherence tomography (OCT). Volume OCT scans were obtained in the macular region of all treated eyes as well as in the peripheral region of subject GD-59.

Tissue preparation

NHP subjects were euthanized and perfused, and their eyes enucleated at 48 days post-injection (ET-79) or 96 days post-injection (FK-34 and GD-59). Retinas from right and left eyes of subject ET-79 and left eyes from subjects FK-34 and GD-59 were used in this study. Briefly, subjects were given sodium heparin (2000 units), then euthanasia was carried out using 64.8 mg/ml sodium pentobarbital (25mg/kg). Access for perfusion was achieved using an intra-aortic cannula inserted through the left ventricle (while the right atrium was cut). Gravity-fed perfusion was initiated using 2 liters of vasodilator solution (0.9% NaCl and 1% $NaNO_2$) followed by 4 liters of fixative (4% paraformaldehyde in 0.1 M Sorensen's phosphate buffer, pH 7.2). The eyes were enucleated with approximately 5 mm of proximal optic nerve retained. Optic nerves from treated and untreated eyes were removed. A slit was made in each cornea, and then eyes/optic nerves were placed into fix buffer for an additional 24 hours at 4°C, then removed and placed into fresh PB buffer (0.1 M Sorensen's phosphate buffer, pH 7.2) and stored at 4°C until sectioning. Peripheral tissues were harvested from the euthanized subject in the following order: right testicle, left testicle, lung, right kidney, left kidney, pancreas, spleen, liver, right submandibular lymph node, left submandibular lymph node, heart, and brain. A fresh, sterile instrumentation pack was used for each organ harvested. Once harvested, the tissues were cut into smaller (in triplicate) pieces with sterile scalpels, flash frozen in liquid nitrogen and stored at −80 until DNA extraction. The brain was also removed at this time, blocked in the coronal plane using a stereotactic device, and placed in PB buffer.

For sectioning, the eyes were dissected to remove the anterior portion of the globe and the vitreous removed. For ET-79, the central retina was divided into three 5-by-8-mm blocks deemed "superior," "macular," and "inferior" (5 mm in superior/inferior axis, 8 mm in nasal temporal axis), such that the GFP-positive bleb was contained wholly within two of the blocks. Using stills from the surgical video and *in vivo* GFP imaging as a guide, we determined visually (using the macula and vasculature pattern as references) that two blocks, the macular and superior, of approximately 5 by 8 mm encompassed the entire region of the bleb and contained ample superior, inferior, nasal, and temporal bleb margins. For FK-34, the central retina was divided into five blocks labeled "superior," "central," "inferior," "temporal," and "nasal," with the bleb encompassed within the central block. For GD-59, the central retina was divided into five blocks labeled "superior", "central", "inferior", "optic disk"

and "nasal" with two blebs extending through the "superior," "central," and "inferior" blocks. Once dissected, the blocks were photographed using a standard dissection microscope. Optic nerves from ET-79 were oriented such that resulting sections were taken in the sagittal plane. Embedding of retina and optic nerve tissue consisted of immersion/equilibration in five different, and successive, solutions: 10% sucrose/PB; 20% sucrose/PB; 30% sucrose/PB; 4 parts 30% sucrose/PB to 1 part HistoPrep (Fisher Scientific, Pittsburgh, PA); and 2 parts 30% sucrose/PB to 1 part HistoPrep. All incubations took place at room temperature for 30 minutes except the 30% sucrose/PB, which took place overnight at 4°C. Once the final incubation was complete, the tissue was placed in 2 parts 30% sucrose to 1 part Histoprep, oriented, and frozen immediately by partial submersion in liquid nitrogen. Embedded retinal blocks from ET-79 were sectioned on the 8 mm axis in an inferior to superior direction for the macula block and superior to inferior direction for the superior block (heading toward the bleb in each case). The central retinal block from FK-34 was sectioned on the 8 mm axis in a superior to inferior direction. FK-34's nasal retinal block was sectioned on the 8 mm axis in a nasal to temporal direction. The superior, central, and inferior retinal blocks from subject GD-59 were sectioned on the 8-mm axis in a superior to inferior direction. All sections were 10 μm thick. Detailed notes were kept during cryosectioning, keeping track of every section pulled and whether or not that section was mounted or discarded, while periodically monitoring the freshly cut sections with the light microscope. Sectioning in this manner allowed for reasonable orientation within the block, keeping in mind that normal variations occur with cutting at 10μm, including expansion and contraction of embedding medium.

Superfrost Plus (Fisher Scientific) slides were used, and the sections were cut on a cryostat (Leica CM3050 S, Wetzlar, Germany) with the cabinet and object temperatures set at −25°C and −15°C, respectively. For brain sections, the brain was equilibrated in 25% sucrose in PB buffer for 96 hours following the perfusion, during which three changes of fresh 25% sucrose in PB buffer occurred. The brains were then sectioned in the coronal plane at 40 μm on a freezing microtome. Sections were stored at 4°C in PB.

Mice were sacrificed immediately after imaging. Treated and untreated eyes were enucleated and placed immediately in 4% paraformaldehyde. All eyes were prepared for cryosectioning as previously described (Haire *et al.*, 2006). Eyecups were serially sectioned at 10 μm with a cryostat (Leica CM3050 S).

Immunohistochemistry and microscopy

NHP retina and optic nerve cryosections were washed three times with 1× PBS (15 minutes each). Samples were then incubated in 0.5% Triton ×-100 for 1 hour in the dark at room temperature and blocked in a mixture of 10% goat serum in 1× PBS for 1 hour at room temperature. Retina samples were then incubated with a rabbit polyclonal antibody raised against primate cone arrestin ("Lumif," generously provided by Dr. Cheryl Craft, University of Southern California) diluted 1:30,000 in a solution containing 1% NHP serum in 1× PBS (serum was isolated from our NHP subjects prior to injection procedure) for approximately 12 hours at 4°C. Samples were then washed three times with 1× PBS (10 minutes each) and incubated for 1 hour at room temperature, with an IgG secondary antibody tagged with Alexa-594 fluorophore (Molecular Probes, Eugene, OR) diluted 1:500 in a mixture of 1× PBS containing 3% NHP serum (the same serum used for primary incubation). Autofluorescence eliminator reagent (Cat. #2160; EMD Millipore, Billerica, MA) was also applied to retinal sections from FK-34 and GD-59. Samples were counterstained with 4',6'-diamidino-2-phenylindole (DAPI) for 5 minutes at room temperature. After a final rinse with 1× PBS, samples were mounted in an aqueous-based media (DAKO) and coverslipped. Optic nerves of ET-79 were counterstained with DAPI only.

Cryosections located within the parafovea were selected based on a previous study that delineated photoreceptor topography of the retina in *Macaca nemestrina* (Packer *et al.*, 1989) and the careful notes we kept during cryosectioning (see Methods). Two retinal sections representing proximal and distal parafoveal retina (located 550 and 850 microns superior to the foveal pits, respectively) of all subjects were selected for analysis. A schematic of photoreceptor topography adapted from Packer *et al.*(1989), along with the locations selected for analysis, are shown in Figure 1.

Mouse retina sections were immunostained according to previously described methods (Boye *et al.*, 2010) with minor modifications. Samples were incubated with a rabbit polyclonal antibody raised against GFP diluted 1:1000 in 0.3% Triton/1% BSA for 12 hours at 4°C. Samples were then washed and incubated in IgG secondary antibody tagged with Alexa-488 (Molecular Probes) diluted 1:500 in 1× PBS

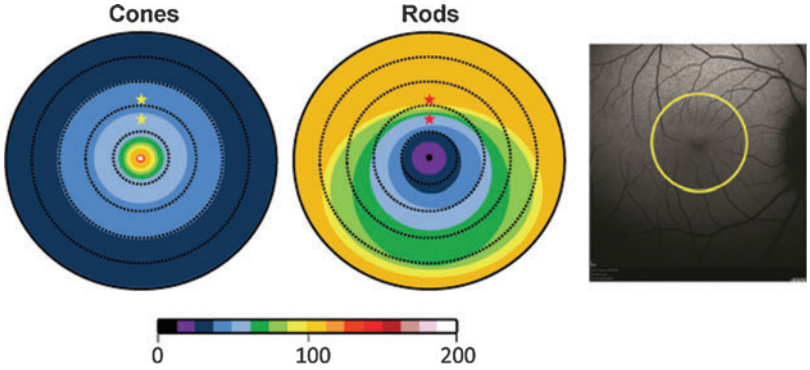

FIG. 1. Schematic representation of cone (left) and rod (right) photoreceptor topography in *Macaca nemestrina* retina using a color scale to reflect average photoreceptor densities at various eccentricities from the foveal pit. Dashed rings are spaced 370 μm apart. Color scale spans the range of 0–200,000 photoreceptors/mm^2. Stars are placed in the two parafoveal retinal regions ("proximal parafovea" −550 μm superior to foveal pit and "distal parafovea" −850 μm superior to foveal pit), which were chosen for immunohistochemical analysis. A Spectralis fundus image of *Macaca nemestrina* is shown on the right with a yellow ring representing the outermost eccentricity of the figures on left.

for 1 hour at room temperature. Secondary-only controls were performed on both mouse and NHP retinal sections.

All NHP and mouse sections were analyzed using spinning disk confocal microscopy (Nikon Eclipse TE2000 microscope equipped with Perkin Elmer Ultraview Modular Laser System and Hamamatsu O-RCA-R2 camera). Raw GFP (NHP sections) or Alexafluor-488 fluorescence (mouse sections) were detected with a 488-nm laser line. Cone arrestin (Alexafluor-594) fluorescence was detected in NHP with a 561 nm laser line. DAPI fluorescence was detected with a 405-nm laser line. Images of all fluorochromes (or raw GFP) were obtained sequentially using either 20× (air) or 40× (oil) objective lenses. All settings (exposure, gain, laser power) were identical for the 20× or 40× objectives, respectively, with one exception. The 488 exposure alone was slightly reduced when capturing the 20× image closest to the injection site in ET-79. Because it was likely exposed to the highest concentration of vector, the GFP signal in this area of the retina was strongest, hence the need for a slight reduction in exposure.

Representative areas of NHP retinas were chosen for analysis; ET-79: 1) foveal pit, 2) proximal parafovea-550 μm superior to foveal pit, 3) distal parafovea-850 μm superior to foveal pit, 4) center of the bleb near injection site, 5) the macular edge of injection bleb, 6) the superior edge of injection bleb, and 7) area outside of the injection bleb; FK-34: 1) foveal pit, 2) parafovea-550 μm superior to foveal pit, 3) distal parafovea-850 μm superior to foveal pit, 4) periphery of central bleb; GD-59: 1) foveal pit, 2) parafovea-550 μm superior to foveal pit, 3) distal parafovea-850 μm superior to foveal pit, 4) periphery of central bleb, 5) center of peripheral bleb. Locating specific areas was based on extensive notes taken during the sectioning process. Care was taken to orient each NHP block using retinal vasculature as a landmark during sectioning. These landmarks were compared to Spectralis images to facilitate orientation. All image analysis was performed using Volocity 5.5 software (PerkinElmer, Waltham, MA). Point spread functions (PSFs) for DAPI, 488 and 594, were generated for deconvolution (iterative restoration) of NHP images at a 95% confidence interval and an iteration limit of 20. Snapshots of final images were exported in .tiff format.

Biodistribution

The spread of vector DNA in tissues of the treated NHPs were determined in samples collected at sacrifice according to previously described methods with modifications (Jacobson *et al.*, 2006b). A major difference between our study and those previously reported is that the biodistribution data reported here was generated from tissue recovered from a perfused animal. All tissues examined in this NHP study were, therefore, exposed to fixative prior to genome recovery. In addition, data generated from all treated subjects and untreated retina (ET-79 only), as well as optic nerves from treated and untreated eyes, was recovered from ≤ 0.10 μg of total genomic DNA. This DNA was extracted from retina and optic nerve tissue removed from those slides that were not used for immunostaining. Approximately six retinal sections (10 microns thick and ~ 1 cm in length) were used for extraction of 0.05 μg of total retinal DNA. Approximately eight sagittal sections of optic nerve (10 microns thick, ~ 1 cm by ~ 0.5 cm) were used for extraction of 0.10 μg of total optic nerve DNA. Genomic DNA extraction and quantitative polymerase chain reactions (PCRs) were performed as previously described (Jacobson *et al.*, 2006b; Song *et al.*, 2002) with minor modifications. Primer pairs were designed to the SV40 poly-adenylation signal (SV40 polyA) region in each vector genome, and standard curves established using known concentrations of plasmid DNA containing the same SV40 polyA target sequence. DNA from all tissues (three samples per periperhal organ and one sample for eyes and optic nerves) was assayed in triplicate. For ET-79, biodistribution was performed on the lateral geniculate nucleus (LGN) as a whole (value shown is the average of bilateral analysis), whereas LGN was divided into right and left quadrants for FK-34 and GD-59.

Neutralizing antibody assays

ARPE-19 cells (purchased from ATCC, Manassas, VA) were routinely maintained in a culture medium consisting of Dulbecco's modified Eagle's medium (DMEM)—Nutrient Mixture F-12, 1:1 mixture with Hepes buffer containing 10% fetal bovine serum (FBS), 0.384% (w/v) additional sodium bicarbonate, 1% 200 Mm L-glutamine, and 50 mg/ml Gentamicin. Cells were incubated at 37°C in 7% CO_2.

NHP serum samples and naive serum from a mouse were heat-inactivated at 56°C for 35 minutes. Self-complimentary AAV5-smCBA-mCherry vector (10^4 genomic copies per cell) was diluted in serum-free DMEM/F-12 1:1 modified medium and incubated with 2-fold serial dilutions (from 1:10 to 1:1280) of heat-inactivated serum samples in DMEM/F-12 1:1 modified medium for 1 hour at 37°C. The serum-vector mixture was then used to infect ARPE-19 cells seeded in 96-well plates containing 3×10^4 cells/well for 1 hour. After 1 hour incubation, an equal volume of 20% FBS DMEM/F-12 1:1 modified medium was added to each well and incubated for 72 hours at 37°C in 7% CO_2 (Calcedo *et al.*, 2009). Three days post-infection, cells were observed under a fluorescent microscope (Olympus IX 70 Inverted Fluorescent Microscope equipped with a QImaging Retiga 4000R Camera with RGB-HM-5 Color Filter and QImaging QCapure Pro 6.0 software; QImaging, Surrey, Canada). All images were taken at identical exposure settings and magnification. Cells were then dissociated with Accutase solution (MP Biomedicals, Solon, OH), and 10,000 cells per sample were counted and analyzed using a BD LSR II flow cytometer equipped with BD FACSDIVA 6.2 software (BD Biosciences, San Jose, CA). mCherry fluorescence was quantified with a PE-Texas-Red-A filter with an excitation wavelength of 532 nm and an emission band pass of 600–620 nm. The transduction efficiency was calculated by multiplying the percentage of cells positive for mCherry by the mean fluorescence intensity (Pajusola *et al.*, 2002; Ryals *et al.*, 2011a). The neutralizing antibody (NAb) titer was reported as the highest serum dilution that inhibited self-complementary AAV5-smCBA-mCherry transduction (mCherry expression) by $\geq 50\%$, compared with mouse naive serum control (Sigma S3509).

Results

Subretinal injections

Injections were carried out using identical instrumentation, devices, and surgical techniques employed in human

vitreoretinal surgery so as to accurately reflect the conditions that would be encountered in future clinical trials. Animal ET-79 had a vitrectomy followed by injection needle placement superior-temporal so that vector injection propagated the detachment toward the macula. The surgical protocol in animal FK-34 was intended to replicate the injection/results of ET-79 and had a minimal vitrectomy followed by injection needle placement slightly superior-temporal to the macula whereby vector injection propagated the detachment toward the macula (~half the volume of ET-79). Animal GD-59 was intended to evaluate transduction in both the peripheral and central retina using two injections, one located peripherally and one centrally. Additionally, a Lambert subretinal needle was evaluated as an alternate injection device. During the initial vitrectomy, animal GD-59 experienced slight surgical-related trauma to the superior retina. A bipolar cautery (Synergetics, O'Fallon, MO) was utilized to repair vessel bleeding.

In life imaging

To initially assess the expression pattern of subretinally-delivered, serotype 5 AAV vector containing the hGRK1 promoter-driving GFP expression in the primate retina *in vivo*, Spectralis images were taken in the Scanning Laser Ophthalmoscope (SLO) 488 nm autofluorescent mode. Imaging time points and findings are summarized in Table 2. Subject ET-79 was imaged at 3 (data not shown) and 5 weeks post-injection (Figs. 2 and 3). Subjects FK-34 and GD-59 were imaged at 2.5 (data not shown) and 5 weeks post injection (Fig. 4). Comparison of the video still image of the subretinal vector bleb at the time of surgery and SLO of subject ET-79 at 5 weeks post-injection revealed that vector-mediated GFP expression was confined to that portion of the retina that was detached during the subretinal injection procedure (Fig. 2). OCT scans through representative areas of the injection blebs of subjects ET-79 and FK-34 were generally unremarkable except for some limited cellular disorganization at the immediate injection site and a small area of abnormal reflectivity in a focal region of the fovea at the level of photoreceptor inner/outer segments (IS/OS) and the retinal pigment epithelium (RPE) (ET-79) (Figs. 3 and 4). With the exception of this reflectivity, there was no gross pathology apparent in any of the primate maculas (central blebs) following vector injection. Representative OCT scans from the superior, central (foveal pit) and inferior macula of the primate eye taken 1 week before and 5 weeks after subretinal injection were similar and exhibited normal retinal thickness and lamination (Fig. 3). GFP expression was present in both the central and peripheral retina of subject GD-59, with fluorescence again confined to the limits of each injection bleb. A retinal hemorrhage created during subretinal surgery temporal/superior to the fovea is also evident (Fig. 4). Again, except for limited disorganization at the injection site within the central bleb (Fig. 4, line 1), OCT scans did not reveal any pathology in the central or peripheral retina of subject GD-59 (Fig. 4, Supplementary Fig. S1; Supplementary Material available online at www.liebertonline.com/hum).

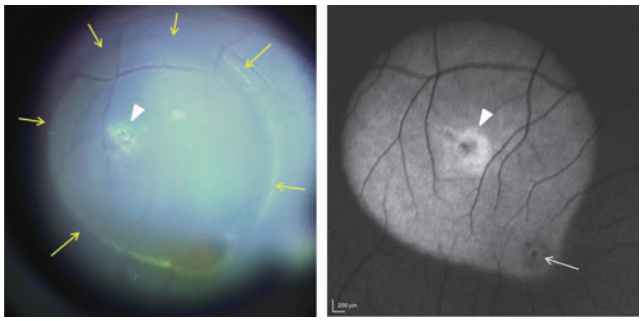

FIG. 2. Subretinal injection bleb and fluorescent fundus image at 5 weeks post-injection with AAV5-hGRK1-GFP in ET-79. Left panel: Yellow arrows in a still photo from the subretinal injection video denote the limits of the 60 μl injection bleb created during vector administration. Right panel: Green fluorescent protein (GFP) fluorescence was detected by 488 nm Spectralis imaging. The macula is indicated with a white arrow. The injection site is indicated with arrowheads in both panels. Scale bars = 200 μm.

With the exception of the area proximal to the injection site of subject ET-79, which exhibited the highest relative fluorescence, GFP expression appeared homogeneous throughout the injection bleb (Figs. 2, 3, and 5). In contrast, the central macular blebs created in subjects FK-34 and GD-59 produced a radial spokelike pattern of GFP expression (Fig. 4). This pattern of GFP fluorescence was evident in the 488 Spectralis images of both monkeys as well as in retinal cross sections from these areas (Fig. 4, Supplementary Fig. S2) and was not evident in the peripheral retina of subject GD-59. Given these GFP fluorescent spokes follow no distinct anatomical or cellular pattern, we postulate that this pattern of GFP expression is the result of an initial reattachment of the central retina in a undulating pattern

Table 2. *In Vivo* Imaging Details

ET-79	5 days pre-injection	20 days post-injection: GFP signal in bleb	39 days post-injection: strong GFP signal in bleb	N/A
FK-34	186 days pre-injection 6 days pre-injection	14 days post-injection: slight GFP signal peripheral to macula	33 days post-injection: strong GFP signal in and around macula	63 days post-injection: strong GFP signal in and around macula
GD-59	186 days pre-injection 6 days pre-injection	14 days post-injection: slight GFP signal in periphery and macula superior temporal shows injection-related damage	33 days post-injection: strong GFP signal in periphery and macula	63 days post-injection: strong GFP signal in periphery and macula

GFP, green fluorescent protein.

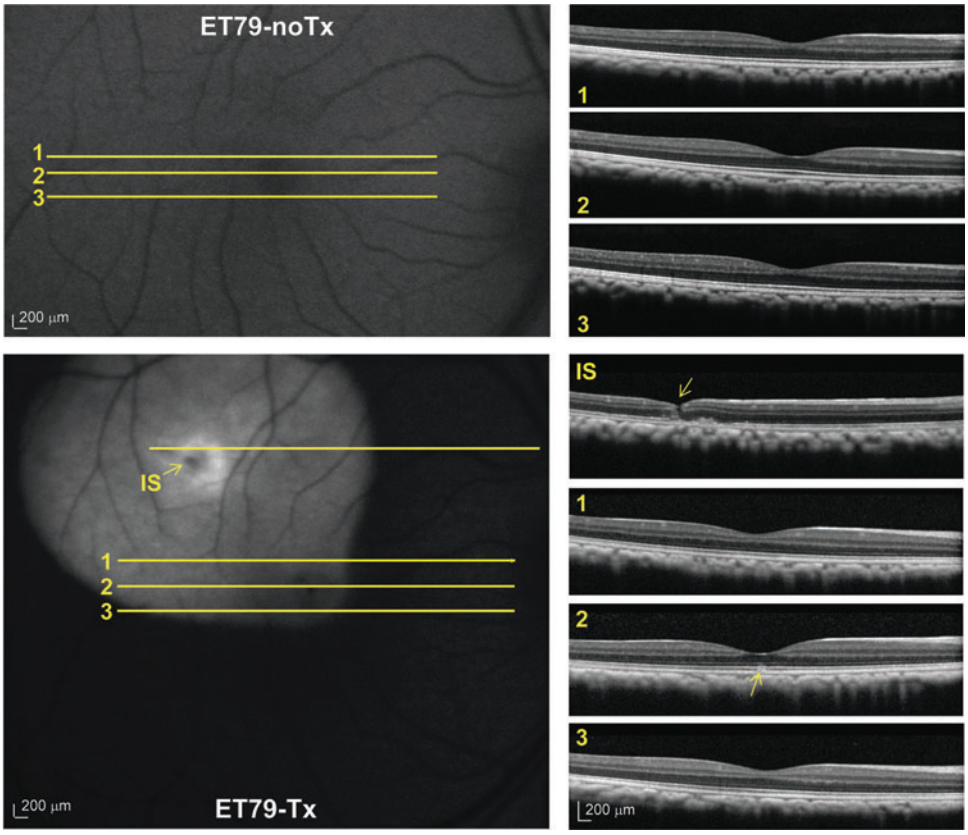

FIG. 3. Pre-and post-injection fluorescent fundus images and corresponding OCT scans in the retina of ET-79. Representative OCT scans corresponding to superior macula (scan 1), foveal pit (scan 2) and inferior macula (scan 3) taken 5 days before (top panel) and 39 days after (bottom panel) AAV5-hGRK1-GFP injection. An additional OCT scan is shown through an area near the injection site (IS) in the bottom panel. The injection needle track is indicated by a yellow arrow (bottom panel, IS). Small changes in reflectivity at the layer of photoreceptor IS/OS and RPE are denoted with a yellow arrow (bottom panel, scan 2). OCT, optical coherence tomography; IS, injection site. Scale bars = 200 μm. Color images available online at www.liebertpub.com/hum

creating a channeling effect of the vector solution. In humans with subretinal detachments, it is not uncommon to observe undulations of the retina during such initial retinal reattachments (D. Witherspoon, personal communication, 2011). Furthermore, we speculate that this observation, revealed through the highly sensitive Spectralis imaging system, may be an unappreciated phenomenon with respect to vectors delivered subretinally. The darker appearance of the primate macula in the autofluorescence imaging mode of the Spectralis (most evident in the foveal pits of subjects ET-79

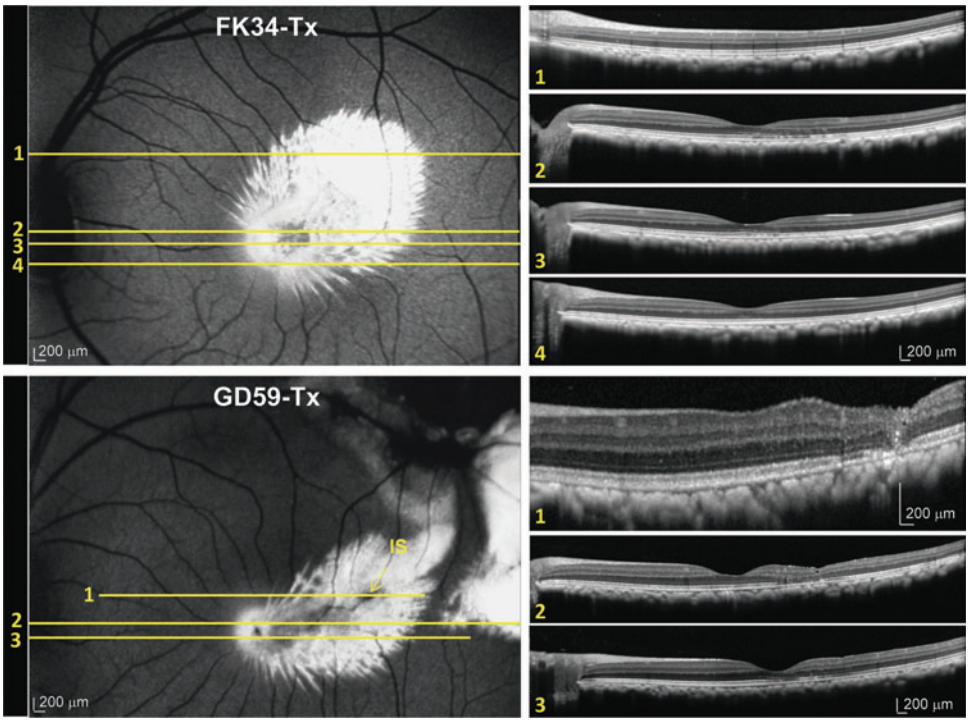

FIG. 4. Post-injection fluorescent fundus images and corresponding OCT scans in nonhuman primate (NHP) subjects FK-34 (top) and GD-59 (bottom). Top Panel: Representative OCT scans corresponding to a superior region of the vector bleb (scan 1), the superior macula (scan 2), the foveal pit (scan 3), and the inferior macula (scan 4) taken 5 weeks after AAV5-hGRK1-GFP injection in subject FK-34. Bottom Panel: Representative OCT scans corresponding to the injection site (IS) in a superior region of central vector bleb (scan 1), the foveal pit (scan 2), and the inferior macula (scan 3) taken from subject GD-59 5 weeks post-injection. Small changes in lamination are visible at IS. Scale bars = 200 μm. Color images available online at www.liebertpub.com/hum

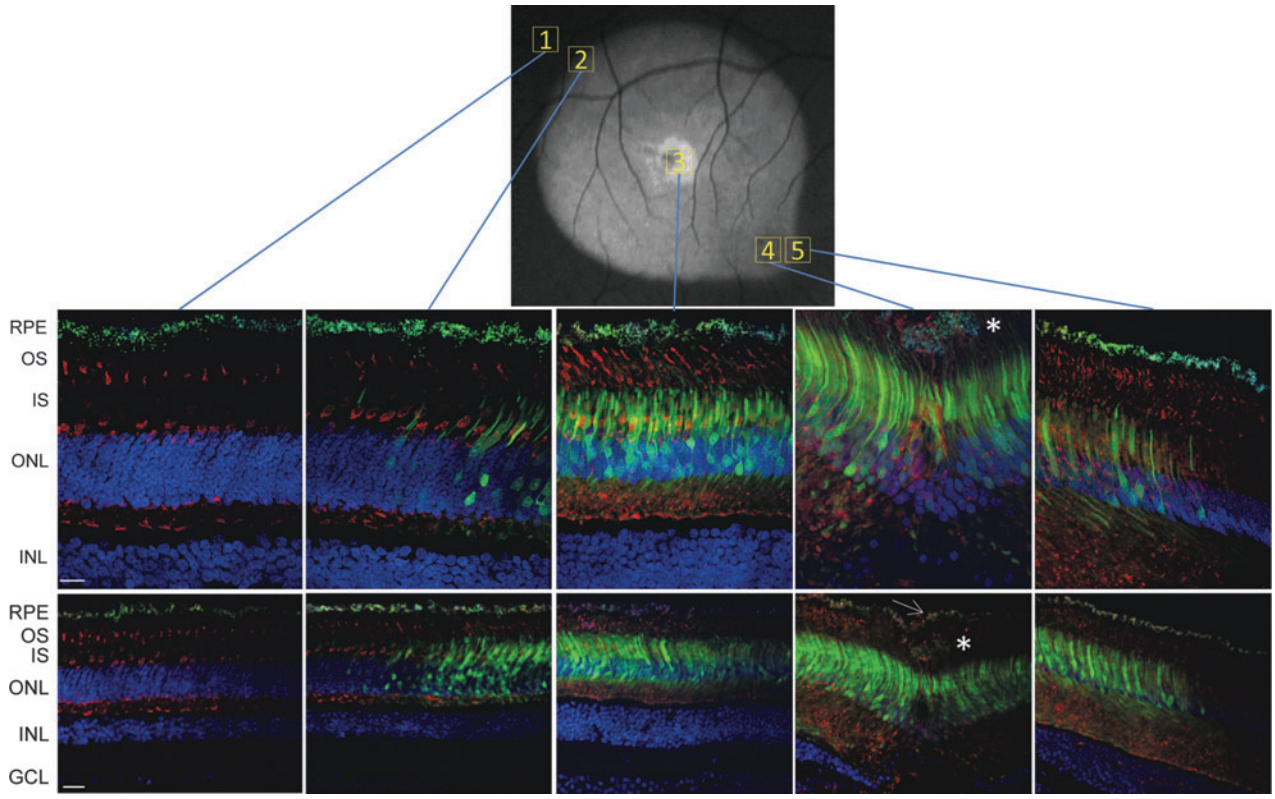

FIG. 5. AAV5-hGRK1-mediated GFP expression in rod and cone photoreceptors of ET-79. **(A)** Cross sections of retina from outside the injection bleb (1), the superior edge of injection bleb (2), injection site (3), foveal pit (4), and macular edge of injection bleb (5) immunostained for cone arrestin (red) and counterstained with DAPI (blue). GFP was detected with its intrinsic fluorescence (green). The Spectralis fundus image is shown for reference (top). Confocal images are shown at 40× (top row) and 20× (bottom row) magnification. Abnormal cells are denoted with asterisk in 20× and 40× foveal pit images. The intact RPE monolayer is denoted with a white arrow in the 20× foveal pit image. Scale bar at 40× = 15 μm; scale bar at 20× = 30 μm. DAPI, 4′,6′-diamidino-2-phenylindole; RPE, retinal pigment epithelium, OS, outer segments, IS, inner segments, ONL, outer nuclear layer, INL, inner nuclear layer.

and GD-59 in Figs. 3 and 4), is a typical observation and, as our immunostaining data shows (Figs. 5 and 6), does not denote a reduction in GFP expression. This darkening is thought to be due to the increased concentration of pigment in this region (Snodderly *et al.*, 1984a). The maximum absorbance of these pigments is 460 nm (Snodderly *et al.*, 1984b), which interferes with the 488 nm excitation light resulting in a reduced fluorescence intensity from vector-transduced cells in these regions. Higher exposure images taken of the right (pre-injection) and left (untreated) eyes of subject ET-79 show this macular feature more clearly (Supplementary Fig. S3).

Immunohistochemistry

AAV5-hGRK1-mediated GFP expression was then evaluated at higher resolution in representative areas of the injected primate retinas. Notably, the vast majority of photoreceptors within the rod-free foveal pit were GFP-positive and, as expected, all cells were positive for cone arrestin (Fig. 6). Upon removal of the blue (DAPI) and red (cone arrestin) channels in the image (Fig. 5), GFP fluorescence is apparent in most, if not all, cone cell bodies in the foveal pits in all three NHP subjects. This finding demonstrates that despite the existence of additional rhodopsin kinase isoforms in cones (Weiss *et al.*, 2001), hGRK1 is active in primate cones. Vector- mediated GFP expression was detected in foveal (Figs. 5 and 6), proximal parafoveal (Fig. 7), and distal parafoveal (Supplementary Fig. S4) cones of all NHP subjects. White arrows denote GFP-positive parafoveal cones at 550 and 850 μm superior to foveal pits of all NHP subjects (Fig. 7 and Supplementary Fig. S4). At 40× magnification, it is clear that cells that appear morphologically to be cones in the parafovea also express cone arrestin, thus confirming their identity (Fig. 7 and Supplementary Fig. S4). Immunohistochemical analysis revealed that GFP expression was confined to photoreceptors within the injection bleb, confirming our *in vivo* imaging results. This result is consistent with previous studies in which AAV5-mediated GFP expression was restricted to the injection bleb of subretinally injected rats (Provost *et al.*, 2005; Stieger *et al.*, 2008). Images of cross sections chosen from the superior and macular edge of the bleb (Fig. 5, fields 2 and 5, respectively) define the boundaries of detectable GFP fluorescence in subject ET-79. Additional images of the edges of detectable GFP expression and just beyond it, taken at equal exposure, are shown in Supplementary Figure S5. GFP expression was also detected in rod photoreceptors, as evidenced by the expression patterns observed in more peripheral retinal cross sections dominated by rods (Fig. 5, field 2, and Fig. 8). The vast

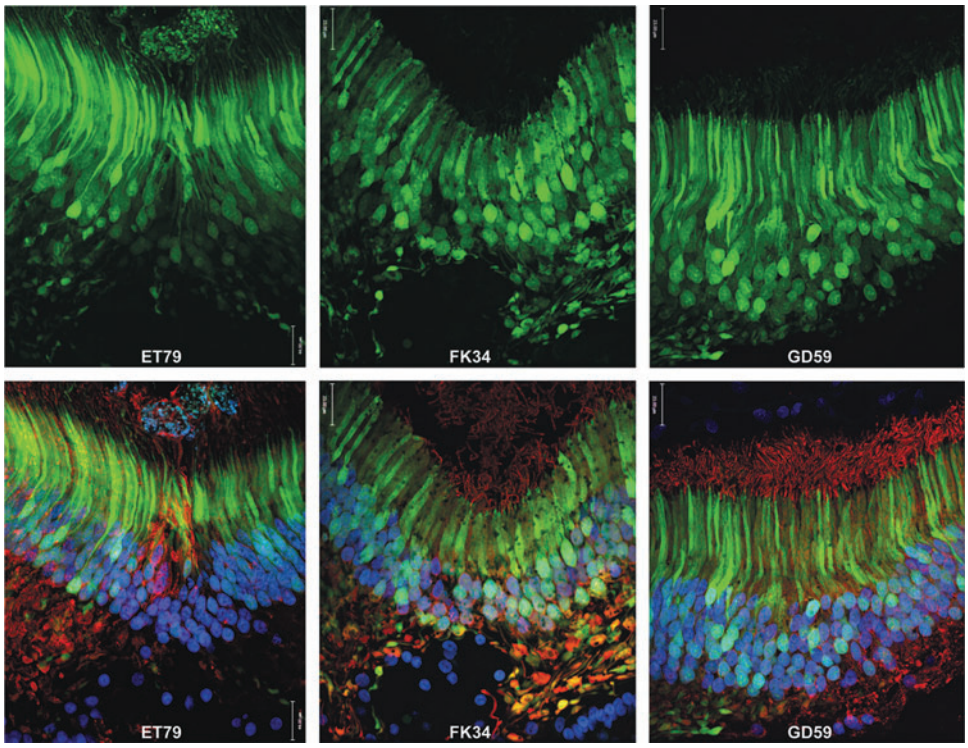

FIG. 6. AAV5-hGRK1-mediated GFP expression in foveal cones of NHP retinas. Cross sections of foveal pits of all NHP subjects (left: ET-79; middle: FK-34; right: GD-59). Images of GFP fluorescence (green) are shown on top. Images of GFP fluorescence (green), cone arrestin immunofluorescence (red), and DAPI nuclear stain (blue) are shown below. Confocal images are shown at 40× magnification. Scale bar = 22 μm.

majority of cell bodies in these rod-rich peripheral sections are GFP positive and negative for cone arrestin. Thus, most of these transduced cells must be rods. GFP was expressed exclusively in cones and rods of all NHP subjects. RPE autofluorescence appeared in all channels in both treated and untreated eyes of subject ET-79 (Figs. 5, 7, and 8; Supplementary Figs. S4–6). To reduce this artifact, autofluorescence eliminator reagent was applied to all retinal cross sections of the second and third subsequent subjects, FK-34 and GD-59. This eliminated all autofluorescence in the RPE cell layer. Analysis of retinal tissue outside the bleb of subject ET-79 revealed an absence of AAV5-hGRK1-mediated transgene expression (Fig. 5, field 1). As expected, no GFP expression was found in the untreated, contralateral control eye of subject ET-79 (Supplementary Fig. S6). Control staining with goat anti-rabbit 594 secondary alone validated the cone arrestin antibody specificity (Supplementary Fig. S6).

In order to compare transduction of an identical vector preparation at the same dose across species (NHP versus mouse), we subretinally injected the same vector preparation into the mouse (Supplementary Fig. S7). Consistent with our results in NHP, GFP expression was seen in the vast majority of photoreceptors (cell bodies, inner/outer segments) within the injection bleb (Supplementary Fig. S7).

Biodistribution

Vector genome (vg) biodistribution studies were performed on injected NHPs to establish whether AAV5-delivered vector DNA was present in the following tissues: treated retina inside and outside injection bleb, untreated retina, optic nerve, brain, testis, kidney, pancreas, spleen, liver, submandibular lymph node (SMLN) and heart (Table 3). As expected, a high amount of vector genomes were recovered from retinal tissue within the injection blebs of all NHP subjects (ranging from 245,635 to 908,490 vg/μg DNA). Relatively low numbers of genomes were recovered from retinal tissue outside the injection bleb (ranging from undetectable to 1695 vg/μg DNA), optic nerves (ranging from 110 to 3020 vg/μg DNA) of the injected eyes, and select portions of brain. Despite the existence of vector genomes in these areas, no transgene expression was detected in retinal tissue outside the bleb (Fig. 5) or in optic nerves of the treated eyes (data not shown). No vector genomes were detected in the untreated retina of subject ET-79 (untreated retinas from FK-34 and GD-59 were not analyzed) or their optic nerves (all subjects). All peripheral tissues were negative for AAV5-delivered sequence with the exception of subject FK-34's spleen, which was near the limit of detection (100 vg/μg DNA).

Neutralizing Antibody

All NHP subjects were screened for the existence of NAbs to AAV5 in serum with an assay using self-complimentary AAV5-smCBA-mCherry and the ARPE-19 ocular cell line, previously shown to be efficiently tranduced by AAV5 vectors (Ryals *et al.*, 2011b). Using FACs to score relative mCherry expression in ARPE-19 cells infected with scAAV5-smCBA-mCherry in the presence of serial dilutions (ranging from 1:10 to 1:1280) of NHP serum samples, we found that none of the three NHP subjects exhibited detectable NAbs to AAV5 prior to the subretinal injection procedure (all NAb titers $<$1:10) (Table 4). Serum taken from each subject at the time of sacrifice (ET-79- 48 days post-injection, FK-34 and GD-59-96 days post-injection) revealed that subjects ET-790 and FK-34 did not develop NAbs to AAV5 following subretinal injection of AAV5-hGRK1-GFP (NAb titers $<$1:10) (Table 4). However, subject GD-59 did develop NAbs to AAV5, with a titer of 1:640 (Table 4). This subject experienced a retinal hemorrhage during the subretinal surgery,

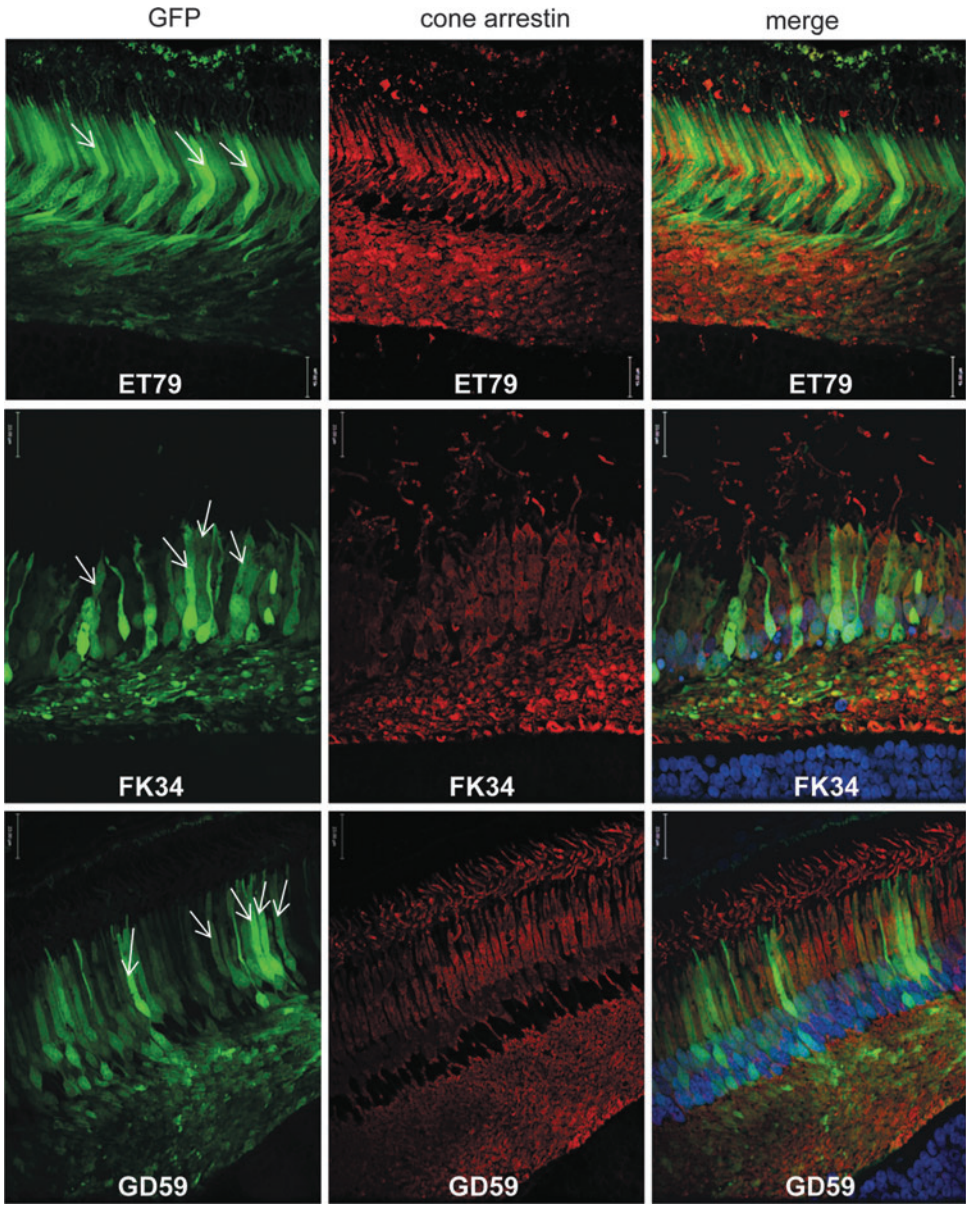

FIG. 7. AAV5-hGRK1-mediated GFP expression in parafoveal cone photoreceptors of NHP retinas. Transverse retinal sections were taken 550 μm superior to the foveal pit in ET-79 (top), FK-34 (middle), and GD-59 (bottom). Left column: GFP fluorescence (green); middle column: cone arrestin immunofluorescence (red); right column: GFP (green), cone arrestin (red), and DAPI nuclear stain (blue). DAPI staining in the retinal section from ET-79 is not visible due to fading over the long storage period. White arrows in the left column indicate several GFP-positive cone photoreceptors exhibiting characteristic cone cell morphology with thick inner segments. Confocal images are shown at 40× magnification. Scale bar = 22 μm.

during which a vector may have gained access to the peripheral vasculature. Coincidently, this subject also received the highest number of total vector genomes (Table 1).

Discussion

This study is the first demonstration that the hGRK1 promoter mediates robust and exclusive transgene expression in both cones and rods of the nonhuman primate retina. The pattern of hGRK1-mediated expression in NHP is consistent with that seen in mouse (Boye *et al.*, 2010; Boye *et al.*, 2011; Khani *et al.*, 2007; Pawlyk *et al.*, 2010; Sun *et al.*, 2010) and is significant given the variability of GRK1 expression in cones across species (Weiss *et al.*, 2001), a recent report that the hGRK1 promoter lacks activity in canine cones (Beltran *et al.*, 2010) and additional studies demonstrating that promoter activities differ across mammalian taxa (Ivanova *et al.*, 2010; Yin *et al.*, 2011) (Boye and Gamlin *et al.*, unpublished results). Despite the many structural differences between the murine and primate retinas, we show that the transduction profile of concentration-matched AAV5-hGRK1-GFP in these two species is comparable. The finding that hGRK1 mediates efficient transgene expression exclusively in NHP photoreceptors following subretinal injection supports incorporation of hGRK1 into AAV vectors designed to treat photoreceptor-mediated diseases in a clinical setting.

A secondary finding of this study is the efficient transduction of both NHP rods and cones following subretinal injection with an AAV5-based vector. This was reproducible in all three subjects injected on two different surgical dates separated by 1 year. While the issue of transducing both rods and cones in an NHP has been investigated previously, results were conflicting and the imaging techniques used to evaluate transduction were less sensitive (Lotery *et al.*, 2003; Mancuso *et al.*, 2007). In 2003, the Davidson lab reported that an AAV5 vector containing the ubiquitous cytomegalovirus

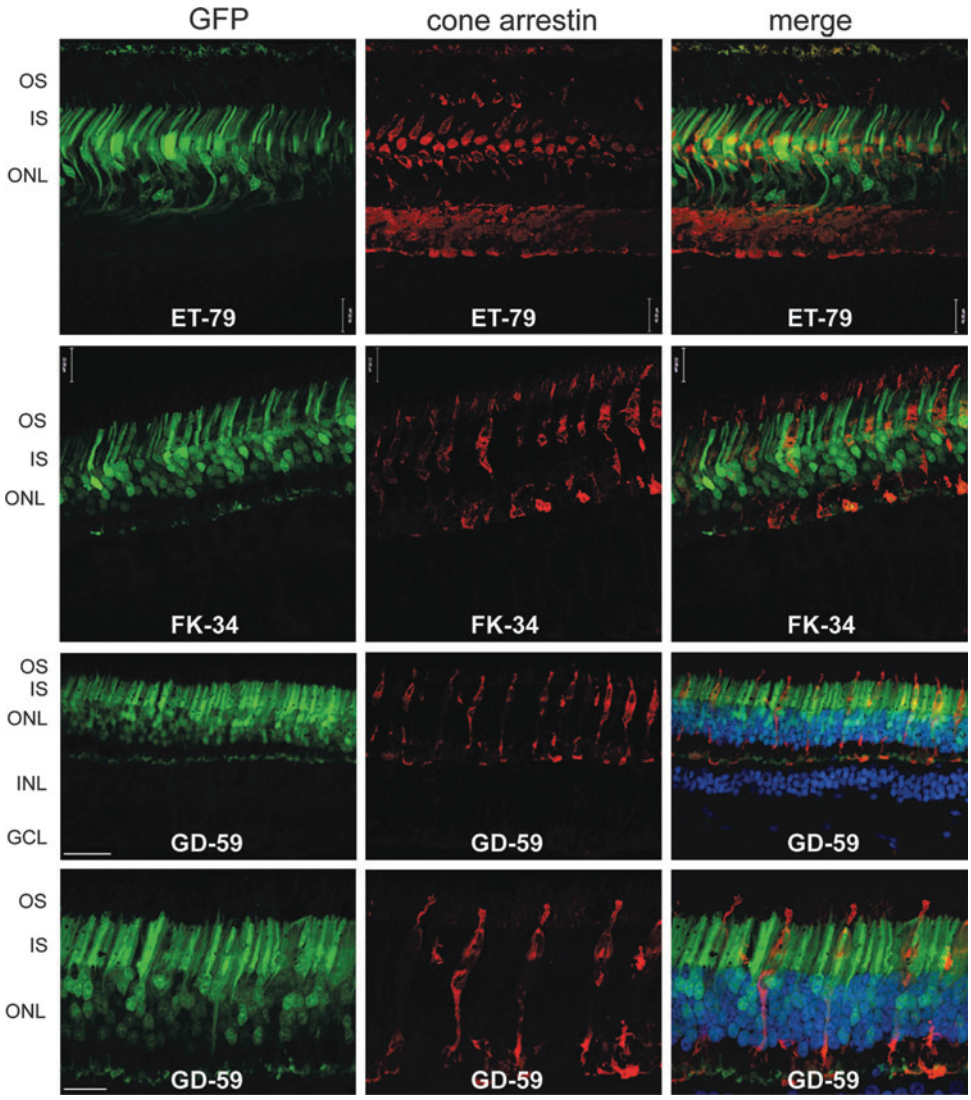

FIG. 8. AAV5-hGRK1-mediated GFP expression in rod photoreceptors of NHP retinas. Cross sections were taken from the periphery of the subretinal vector blebs in ET-79 and FK-34 and from the peripheral subretinal vector bleb of GD-59. Left column: intrinsic GFP fluorescence (green); middle column: cone arrestin immunofluorescence (red); right column: GFP (green), cone arrestin (red), and DAPI nuclear stain (blue). DAPI staining from ET-79 is not visible due to fading over the long storage period. 20× images are shown for ET-79 and FK-34. 20× and 40× confocal images are shown for GD-59. GFP fluorescence is evident in many photoreceptors lacking cone arrestin expression (rods) in peripheral retinal regions of all NHP subjects. Scale bar at 40× = 22 μm; scale bar at 20× = 30 μm. OS, outer segments; IS, inner segments; ONL, outer nuclear layer; INL, inner nuclear layer; GCL, ganglion cell layer.

(CMV) promoter failed to drive GFP expression in cones following subretinal delivery in rhesus or cynomolgus monkeys (Lotery *et al.*, 2003). Attempts were made to transduce cones in multiple anatomical regions, including the macula, at vector doses ranging from $3–12\times10^8$ particles delivered. Postoperative *in vivo* imaging was performed with a Zeiss fundoscope. Immunohistochemical analysis of retinal sections was restricted to cross sections from one monkey that received a subretinal injection in the nasal retina. Key differences between this report and the current study may account for the lack of cone transduction observed, including differences in vector concentration (a higher concentration of 1×10^{12} particles/ml was used in the current study), promoter choice, and postoperative analysis (a more thorough analysis of various retinal regions, including the cone-rich fovea, was performed in the current study). In 2007, the Neitz lab reported that an AAV5 vector containing the CHOPS2053 promoter [a promoter fragment containing two segments of DNA from upstream of the human X-chromosome opsin gene array (Wang *et al.*, 1992), also known as "PR2.1"] drove GFP expression in cones following subretinal delivery in the squirrel monkey (Mancuso *et al.*, 2007). Vector (concentration unreported) was delivered to multiple areas of the retina, including the macula. Postoperative *in vivo* imaging was performed with the RetCamII (Massie Laboratories, Pleasanton, CA). Immunohistochemical analysis of a single retinal cross section located "just inferior to the fovea" revealed GFP-positive cone photoreceptors. The current study improves upon previous reports in that we have utilized state-of-the-art imaging technology to provide a more detailed analysis of AAV5-mediated transduction, both in life with fluorescent Spectralis imaging and OCT imaging and post mortem with confocal microscopy. In addition, we evaluated AAV5-mediated transgene expression more extensively by analyzing retinal cross sections from a variety of retinal areas, including the cone-rich foveal pit and parafovea.

Previously, Beltran *et al.* found that when delivered subretinally to dogs, AAV5-hGRK1-GFP vector, at a dose of 2.27×10^{12} total vector genomes delivered, resulted in cone toxicity (Beltran *et al.*, 2010). AAV5 vectors with the strong hybrid CMV/chicken beta actin (CBA) promoter showed general photoreceptor toxicity (outer nuclear layer thinning) at doses greater than 7.05×10^{11} total vector genomes

Table 3. Detection of rAAV Vector Sequences by Polymerase Chain Reaction in Nonhuman Primate Tissue Samples

	ET-79	*FK-34*	*GD-59*
Retina (R): Tx inside injection bleb	+(908,490)	NA	NA
Retina (R): Tx outside injection bleb	+(675)	NA	NA
Retina (L)	-	+(417,605)	+(246635)
Retina (L): Tx outside injection bleb	NA	-	+(1695)
Optic nerve (R)	+(3020)	-	-
Optic nerve (L)	-	+(510)	+(110)
Anterior chiasm	+(330)	+(133)	+(99)
Chiasm proper	-	+(411)	+(211)
Optic tract (R)	-	-	+(146)
Optic tract (L)	-	+(261)	+(1510)
LGN (R)	+(590)*	+(97)	-
LGN (L)	+(590)*	+(974)	+(170)
Testis (R)	-	-	-
Testis (L)	-	-	-
Kidney (R)	-	-	-
Kidney (L)	-	-	-
Pancreas	-	-	-
Spleen	-	+(104)	-
Liver	-	-	-
SMLN (R)	-	-	-
SMLN (L)	-	-	-
Heart	-	-	-

R, right; L, left; Tx, treatment; −, no PCR amplification; +, PCR amplification of vector sequence (replicated value shown is average, copy number per μg of DNA); *, value shown is average of bilateral analysis; SMLN, submandibular lymph node; LGN, lateral geniculate nucleus.

delivered (Beltran *et al.*, 2010). In our study, we found that AAV5-hGRK1-GFP at a dose of 6.00×10^{10} vector genomes delivered was well tolerated in the NHP retina, with no apparent photoreceptor toxicity, suggesting the upper limit of toxicity must be above this concentration. The vector dose used in the current study falls within the range proven sufficient for restoration of visual function/preservation of retinal structure following AAV5-mediated treatment of multiple mouse and dog models of photoreceptor-mediated, inherited retinal disease (Alexander *et al.*, 2007; Boye *et al.*, 2010; Gorbatyuk *et al.*, 2010; Komaromy *et al.*, 2010; Li *et al.*, 2011; Mao *et al.*, 2011; Min *et al.*, 2005; Pang *et al.*, 2010; Pang *et al.*, 2008; Pang *et al.*, 2012b; Yao *et al.*, 2011). In at least 11 reports, all of which utilized AAV5-based vectors produced by the same laboratory (University of Florida), vectors were delivered to respective animal models at concentrations between 1×10^{9}–4×10^{10} vector genomes delivered. None of these studies incorporated dose de-escalation analysis, suggesting that the minimum therapeutic dose may fall below this range. Notably, AAV5 is the only serotype tested thus far to confer a gain of visual function in an NHP following transduction of retina (Mancuso *et al.*, 2009). In that study, AAV5 containing the L/M cone-specific PR2.1 promoter drove expression of human L-opsin in cones resulting in trichromacy in previously dichromatic male squirrel monkeys. The AAV5-PR2.1-L-opsin vector was delivered subretinally at a dose of $\sim2.7\times10^{13}$ vector genomes delivered. Co injections of AAV5-PR2.1-L-opsin and AAV5-PR2.1-GFP at a dose of 8.9×10^{12} delivered vector genomes were performed in order to visualize regions of transduced retina in life. While a thorough analysis of photoreceptor toxicity was not performed in this study, the treated squirrel monkeys' improvements in color vision remained stable for more than 2 years, suggesting that these vector doses were also well tolerated (Mancuso *et al.*, 2009).

Table 4. Neutralizing Antibody (Nab) Titers of NHP Serum Pre- and Post-subretinal Injection with AAV5

	ET-79	*FK-34*	*GD-59*
Pre-injection	<1:10	<1:10	<1:10
Post-injection	<1:10	<1:10	1:640

In the current study all NHP retinal cross sections observed within and outside the injection bleb(s) appeared morphologically normal. Aside from disorganization proximal to the injection sites, no retinal thinning was observed in any area. Confirming our OCT results from subject ET-79, microscopy of the foveal pit of the injected eye revealed a small clump of cells in the subretinal space (Fig. 5, field 4). They were small in number and exclusive to this area. The pattern of autofluorescence (Fig. 5, field 4) and pigmentation (data not shown) seen in these cells resembled that of the overlying RPE monolayer. It is known that the adult mammalian RPE has the capacity to proliferate under stress conditions such as retinal detachment (Anderson *et al.*, 1981; Fisher *et al.*, 2005) when RPE cells divide and daughter cells migrate from the RPE monolayer to form complex "cellular membranes" in the subretinal space (Fisher *et al.*, 2005). These proliferates may exist independent of an intact overlaying monolayer and, assuming proper polarity, can continue to support photoreceptor outer segment regeneration following reattachment(Fisher *et al.*, 2005).

Studies have shown that the immune response to AAV vectors differs with respect to the route of administration (Anand *et al.*, 2000; Anand *et al.*, 2002; Barker *et al.*, 2009; Li *et al.*, 2008; Li *et al.*, 2009). Here we show that subretinal injection of AAV5 led to generation of neutralizing antibodies (NAb) against vector capsid in one of three NHP subjects. The finding that post-injection serum from NHP subject GD-59 had a neutralizing Ab titer (1:640) could be artifactual because of the retinal hemorrhage that accompanied this injection procedure and/or the increased vector dose delivered to this subject relative to the other two. In the absence of surgical complications (subjects ET-79 and FK-34), neutralizing antibody titers were undetectable. Recent results from one Leber congenital amaurosis-2 (LCA2) clinical trial showed that subretinal injection of AAV2 did produce slight increases in neutralizing antibodies against capsid (Simonelli *et al.*, 2010). However, these levels were not sustained nor did they compromise the efficacy of a second subretinal injection in the contralateral eye (Bennett *et al.*, 2012; Maguire *et al.*, 2008; Simonelli *et al.*, 2010). Similarly, increases in serum NAb titers against AAV2 were documented after subretinal injection in Rpe65 mutant dogs (Amado *et al.*, 2010; Annear *et al.*, 2011) and in NHPs (Amado *et al.*, 2010). Despite these measurable immune responses, the safety and efficacy of a

second subretinal injection was not compromised. While these results are not directly comparable to ours due to differences in vector serotype, injection volumes, NAb assay methodology, and surgical outcomes (they reported no surgical complications, whereas our subject GD-59 experienced a hemorrhage), these authors suggest that generation of NAb titers against vector capsid does not necessarily preclude effective re-administration of vector. Additional studies will be required to establish whether repeat administration of AAV5 will be equally well tolerated.

This study is the first to examine biodistribution of AAV5-delivered vector genomes following subretinal delivery to the NHP eye. Our results are consistent with other studies that reported either minimal or no vector genomes in dog and pig brain following subretinal injection of AAV5 vectors (Mussolino *et al.*, 2011; Provost *et al.*, 2005). Despite detection of genomes in optic nerve/brain of some subjects, AAV-mediated GFP expression was restricted to photoreceptors of the treated eye. Vector genomes were recovered outside the brain (spleen) only in subject FK-34, but at levels near the detection limit of the assay, indicating that the biodistribution pattern is consistent with those reported following subretinal administration of AAV2 (Jacobson *et al.*, 2006b).

Analysis of retinal cross sections located throughout the NHP fovea/macula revealed that AAV5 efficiently transduced rods as well as foveal and parafoveal cones. By inference, we can conclude that AAV5 mediates efficient transduction of all subclasses of cones, since cones of the foveal pit are exclusively M and L cones, and S-cones predominate in the parafoveal ring immediately eccentric to the fovea (Curcio *et al.*, 1991). Our result differs from that reported following subretinal injections of other AAV serotypes (Vandenberghe *et al.*, 2011). When delivered at a dose of 1×10^{10} vg, AAV7, AAV8, AAV9, rh.8R, and rh.64R1 efficiently targeted rods, while only AAV9 and rh.64R1 efficiently transduced foveal cones. Interestingly, AAV9 and rh.64R1 failed to efficiently transduce parafoveal cones (Vandenberghe *et al.*, 2011). Reasons for the differential ability of AAV serotypes to transduce cones in the parafovea remain to be elucidated. A possible explanation may lie in the ability of respective serotypes to transduce S-cones (Curcio *et al.*, 1991). A more thorough analysis of AAV transduction profiles of multiple vector serotypes, coupled with identification of cone subtypes via immunohistochemistry, will be required to address this issue. Nevertheless, gene-targeting to this region will be essential as the earliest loss of function and degeneration often occurs in para/perifoveal photoreceptors as a consequence of both normal aging or a variety of retinal degenerative diseases such as age-related macular degeneration (AMD), Stargardt's disease (STGD), cone/cone-rod dystrophies, achromatopsia, and LCA (Curcio, 2001; Curcio *et al.*, 1996; Goto-Omoto *et al.*, 2006; Owsley *et al.*, 2000; Robson *et al.*, 2004; Cideciyan *et al.*, 2012; Mackay *et al.*, 2011; Okano *et al.*, 2012; Robson *et al.*, 2008a; Robson *et al.*, 2008b; Scholl *et al.*, 2004).

Ongoing clinical trials using an AAV2 vector to deliver *Rpe65* to the retinal pigment epithelium have proven safe and effective (Ashtari *et al.*, 2011; Bainbridge *et al.*, 2008; Bennett *et al.*, 2012; Cideciyan *et al.*, 2008; Hauswirth *et al.*, 2008; Jacobson *et al.*, 2012; Maguire *et al.*, 2008) and have provided an encouraging platform from which many other ocular gene-replacement strategies will likely emerge. However, an approach involving different AAV vectors will certainly be required to target therapeutic genes to cells of the neural retina. Many proof-of-concept studies in animal models of photoreceptor-mediated diseases have begun to address what these vectors might be (Stieger and Lorenz, 2010; Sundaram *et al.*, 2012). The current study adds to this knowledge base and suggests that the hGRK1 promoter, in conjunction with AAV serotype 5, will be an effective modality for targeting therapeutic transgene expression simultaneously to rod and cone photoreceptors in a clinical setting. To our knowledge, this study is the first to describe an AAV vector capable of mediating efficient and exclusive transgene expression in all photoreceptor subclasses of NHP, including those in the parafovea, a senstive retinal region that often exhibits early pathology as a consequence of normal aging and a variety of inherited retinal diseases.

Acknowledgments

The authors would like to thank James Peterson, Debbie Whitten, Deidra Isbell, Myra Rivers, and Tracy Morris for their excellent technical assistance. We also thank Matt Perrine from Alcon for providing outstanding logistical assistance, and Dr. Christine Curcio and Dr. Steve Fisher for their helpful input. We thank Ocular Instruments, Inc., and Volk Optical, Inc., for surgical instrument donations. We acknowledge NIH grants EY13729, EY11123, EY08571, RR025777, P30-EY021721, and grants from the EyeSight Foundation of Alabama, Carl G. and Pauline Buck Trust, Macular Vision Research Foundation, Foundation Fighting Blindness, Eldon Family Foundation, Vision for Children, and Research to Prevent Blindness, Inc., for partial support of this work.

Author Disclosure Statement

W.W.H. and the University of Florida have a financial interest in the use of AAV therapies and own equity in a company (AGTC, Inc.) that might, in the future, commercialize some aspects of this work.

References

Alexander, J. J., *et al.* (2007). Restoration of cone vision in a mouse model of achromatopsia. Nat. Med. 13, 685–687.

Amado, D., *et al.* (2010). Safety and efficacy of subretinal readministration of a viral vector in large animals to treat congenital blindness. Sci. Transl. Med. 2, 21ra16.

Anand, V., Chirmule, N., Fersh, M., *et al.* (2000). Additional transduction events after subretinal readministration of recombinant adeno-associated virus. Hum. Gene Ther. 11, 449–457.

Anand, V., Duffy, B., Yang, Z., *et al.* (2002). A deviant immune response to viral proteins and transgene product is generated on subretinal administration of adenovirus and adeno-associated virus. Mol. Ther. 5, 125–132.

Anderson, D. H., Stern, W. H., Fisher, S. K., *et al.* (1981). The onset of pigment epithelial proliferation after retinal detachment. Invest Ophthalmol. Vis. Sci. 21, 10–16.

Annear, M. J., Bartoe, J. T., Barker, S. E., *et al.* (2011). Gene therapy in the second eye of RPE65-deficient dogs improves retinal function. Gene Ther. 18, 53–61.

Ashtari, M., *et al.*, (2011). The human visual cortex responds to gene therapy-mediated recovery of retinal function. J. Clin. Invest 121, 2160–2168.

Auricchio, A., Kobinger, G., Anand, V., *et al.* (2001). Exchange of surface proteins impacts on viral vector cellular specificity and

transduction characteristics: the retina as a model. Hum. Mol. Genet. 10, 3075–3081.

Bainbridge, J. W., *et al.* (2008). Effect of gene therapy on visual function in Leber's congenital amaurosis. N. Engl. J. Med. 358, 2231–2239.

Barker, S. E., *et al.* (2009). Subretinal delivery of adeno-associated virus serotype 2 results in minimal immune responses that allow repeat vector administration in immunocompetent mice. J. Gene Med. 11, 486–497.

Beltran, W. A., Boye, S. L., Boye, S. E., *et al.* (2010). rAAV2/5 gene-targeting to rods: dose-dependent efficiency and complications associated with different promoters. Gene Ther. 17, 1162–1174.

Beltran, W. A., *et al.* (2012). Gene therapy rescues photoreceptor blindness in dogs and paves the way for treating human X-linked retinitis pigmentosa. Proc. Natl. Acad. Sci. U.S.A 109, 2132–2137.

Bennett, J., *et al.* (2012). AAV2 gene therapy readministration in three adults with congenital blindness. Sci. Transl. Med. 4, 120ra15.

Boye, S. E., *et al.* (2010). Functional and behavioral restoration of vision by gene therapy in the guanylate cyclase-1 (GC1) knockout mouse. PLoS One 5, e11306.

Boye, S. L., *et al.* (2011). Long-term preservation of cone photoreceptors and restoration of cone function by gene therapy in the guanylate cyclase-1 knockout (GC1KO) mouse. Invest Ophthalmol. Vis. Sci. 52, 7098–7108.

Calcedo, R., Vandenberghe, L. H., Gao, G., *et al.* (2009). Worldwide epidemiology of neutralizing antibodies to adeno-associated viruses. J. Infect. Dis. 199, 381–390.

Cideciyan, A. V., *et al.* (2008). Human gene therapy for RPE65 isomerase deficiency activates the retinoid cycle of vision but with slow rod kinetics. Proc. Natl. Acad. Sci. U.S.A, 105, 15112–15117.

Cideciyan, A. V., Swider, M., Aleman, T. S., *et al.* (2012). Macular function in macular degenerations: repeatability of microperimetry as a potential outcome measure for ABCA4-associated retinopathy trials. Invest Ophthalmol. Vis. Sci. 53, 841–852.

Curcio, C. A. (2001). Photoreceptor topography in ageing and age-related maculopathy. Eye (Lond) 15, 376–383.

Curcio, C. A., Allen, K. A., Sloan, K. R., *et al.* (1991). Distribution and morphology of human cone photoreceptors stained with anti-blue opsin. J. Comp. Neurol. 12, 610–624.

Curcio, C. A., Medeiros, N. E., and C. L. Millican. (1996). Photoreceptor loss in age-related macular degeneration. Invest Ophthalmol. Vis. Sci. 37, 1236–1249.

Daya, S., and Berns, K. I. (2008). Gene therapy using adeno-associated virus vectors. Clin. Microbiol. Rev. 21, 583–593.

Dryja, T. (2001). Retinitis pigmentosa and stationary night blindness. In *The Online Metabolic and Molecular Bases of Inherited Disease.* (McGraw Hill, New York).

Fisher, S. K., Lewis, G., Linberg, K. A., *et al.* (2005). Cellular remodeling in mammalian retina: results from studies of experimental retinal detachment. Prog. Retin. Eye Res. 24, 395–431.

Gorbatyuk, M. S., Knox, T., LaVail, M. M., *et al.* (2010). Restoration of visual function in P23H rhodopsin transgenic rats by gene delivery of BiP/Grp78. Proc. Natl. Acad. Sci. U.S.A 107, 5961–5966.

Goto-Omoto, S., Hayashi, T., Gekka, T., *et al.* (2006). Compound heterozygous CNGA3 mutations (R436W, L633P) in a Japanese patient with congenital achromatopsia. Vis. Neurosci. 23, 395–402.

Haire, S. E., Pang, J., Boye, S. L., *et al.* (2006). Light-driven cone arrestin translocation in cones of postnatal guanylate cyclase-1 knockout mouse retina treated with AAV-GC1. Invest Ophthalmol. Vis. Sci. 47, 3745–3753.

Hauswirth, W. W., *et al.* (2008). Treatment of leber congenital amaurosis due to RPE65 mutations by ocular subretinal injection of adeno-associated virus gene vector: short-term results of a phase I trial. Hum. Gene Ther. 19, 979–990.

Ivanova, E., Hwang, G. S., Pan, Z. H., *et al.* (2010). Evaluation of AAV-mediated expression of Chop2-GFP in the marmoset retina. Invest Ophthalmol. Vis. Sci. 51, 5288–5296.

Jacobson, S. G., *et al.* (2006a). Safety of recombinant adeno-associated virus type 2-RPE65 vector delivered by ocular subretinal injection. Mol. Ther. 13, 1074–1084.

Jacobson, S. G., *et al.* (2006b). Safety in nonhuman primates of ocular AAV2-RPE65, a candidate treatment for blindness in Leber congenital amaurosis. Hum. Gene Ther. 17, 845–858.

Jacobson, S. G., *et al.* (2012). Gene therapy for leber congenital amaurosis caused by RPE65 mutations. safety and efficacy in 15 children and adults followed up to 3 years. Arch. Ophthalmol. 130, 9–24.

Khani, S. C., *et al.* (2007). AAV-mediated expression targeting of rod and cone photoreceptors with a human rhodopsin kinase promoter. Invest Ophthalmol. Vis. Sci. 48, 3954–3961.

Komaromy, A. M., *et al.* (2010). Gene therapy rescues cone function in congenital achromatopsia. Hum. Mol. Genet. 19, 2581–2593.

Li, Q., Miller, R., Han, Y., *et al.* (2008). Intraocular route of AAV2 vector administration defines humoral immune response and therapeutic potential. Mol. Vis. 14, 1760–1769.

Li, W., *et al.* (2009). Gene therapy following subretinal AAV5 vector delivery is not affected by a previous intravitreal AAV5 vector administration in the partner eye. Mol. Vis. 15, 267–275.

Li, X., *et al.* (2011). Gene therapy rescues cone structure and function in the 3-month-old rd12 mouse. a model for mid-course RPE65 leber congenital amaurosis. Invest Ophthalmol. Vis. Sci. 52, 7–15.

Lotery, A. J., *et al.* (2003). Adeno-associated virus type 5. transduction efficiency and cell-type specificity in the primate retina. Hum. Gene Ther. 14, 1663–1671.

Mackay, D. S., *et al.* (2011). Screening of SPATA7 in patients with Leber congenital amaurosis and severe childhood-onset retinal dystrophy reveals disease-causing mutations. Invest Ophthalmol. Vis. Sci. 52, 3032–3038.

Maguire, A. M., *et al.* (2008). Safety and efficacy of gene transfer for Leber's congenital amaurosis. N. Engl. J. Med. 358, 2240–2248.

Mancuso, K., Hendrickson, A. E., Connor, Jr., T. B., *et al.* (2007). Recombinant adeno-associated virus targets passenger gene expression to cones in primate retina. J. Opt. Soc. Am. A Opt. Image Sci. Vis. 24, 1411–1416.

Mancuso, K., Hauswirth, W. W., Li, Q., *et al.* (2009). Gene therapy for red-green colour blindness in adult primates. Nature 461, 784–787.

Mao, H., James, Jr., T., Schwein, A. *et al.* (2011). AAV delivery of wild-type rhodopsin preserves retinal function in a mouse model of autosomal dominant retinitis pigmentosa. Hum. Gene Ther. 22, 567–575.

Min, S. H., *et al.* (2005). Prolonged recovery of retinal structure/function after gene therapy in an Rs1h-deficient mouse model of x-linked juvenile retinoschisis. Mol. Ther. 12, 644–651.

Mussolino, C., *et al.* (2011). AAV-mediated photoreceptor transduction of the pig cone-enriched retina. Gene Ther. 18, 637–645.

Okano, K., *et al.* (2012). Retinal cone and rod photoreceptor cells exhibit differential susceptibility to light-induced damage. J. Neurochem. 121, 146–156.

Owsley, C., Jackson, G. R., Cideciyan, A. V., *et al.* (2000). Psychophysical evidence for rod vulnerability in age-related macular degeneration. Invest Ophthalmol. Vis. Sci. 41, 267–273.

Packer, O., Hendrickson, A. E., and Curcio, C. A. (1989). Photoreceptor topography of the retina in the adult pigtail macaque (Macaca nemestrina). J. Comp Neurol. 288, 165–183.

Pajusola, K., Gruchala, M., Joch, H., *et al.* (2002). Cell-type-specific characteristics modulate the transduction efficiency of adeno-associated virus type 2 and restrain infection of endothelial cells. J. Virol. 76, 11530–11540.

Pang, J., *et al.* (2010). Self-complementary AAV-mediated gene therapy restores cone function and prevents cone degeneration in two models of Rpe65 deficiency. Gene Ther. 17, 815–826.

Pang, J. J., *et al.* (2008). AAV-mediated gene therapy for retinal degeneration in the rd10 mouse containing a recessive PDE-beta mutation. Invest Ophthalmol. Vis. Sci. 49, 4278–4283.

Pang, J. J., *et al.* (2012a). AAV-mediated cone rescue in a naturally occurring mouse model of CNGA3-achromatopsia. PLoS. One. 7, e35250.

Pang, J. J., *et al.* (2012b) AAV-mediated cone rescue in a naturally occurring mouse model of CNGA3-achromatopsia. PLoS. One. 7, e35250.

Pawlyk, B. S., *et al.* (2010). Replacement gene therapy with a human RPGRIP1 sequence slows photoreceptor degeneration in a murine model of Leber congenital amaurosis. Hum. Gene Ther. 21, 993–1004.

Provost, N., *et al.* (2005). Biodistribution of rAAV vectors following intraocular administration: evidence for the presence and persistence of vector DNA in the optic nerve and in the brain. Mol. Ther. 11, 275–283.

Robson, A. G., Egan, C. A., Luong, A., *et al.* (2004). Comparison of fundus autofluorescence with photopic and scotopic fine-matrix mapping in patients with retinitis pigmentosa and normal visual acuity. Invest Ophthalmol. Vis. Sci. 45, 4119–4125.

Robson, A. G., Michaelides, M., Luong, A., *et al.* (2008a). Functional correlates of fundus autofluorescence abnormalities in patients with RPGR or RIMS1 mutations causing cone or cone rod dystrophy. Br. J. Ophthalmol. 92, 95–102.

Robson, A. G., Michaelides, M., Saihan, Z. *et al.* (2008b). Functional characteristics of patients with retinal dystrophy that manifest abnormal parafoveal annuli of high density fundus autofluorescence; a review and update. Doc. Ophthalmol. 116, 79–89.

Ryals, R. C., Boye, S. L., Dinculescu, A., *et al.* (2011a). Quantifying transduction efficiencies of unmodified and tyrosine capsid mutant AAV vectors in vitro using two ocular cell lines. Mol. Vis. 17, 1090–1102.

Ryals, R. C., Boye, S. L., Dinculescu, A., *et al.* (2011b). Quantifying transduction efficiencies of unmodified and tyrosine capsid mutant AAV vectors in vitro using two ocular cell lines. Mol. Vis. 17, 1090–1102.

Scholl, H., Chong, N. H., Robson, A. G., *et al.* (2004). Fundus autofluorescence in patients with leber congenital amaurosis. Invest Ophthalmol. Vis. Sci. 45, 2747–2752.

Simonelli, F., *et al.* (2010). Gene therapy for Leber's congenital amaurosis is safe and effective through 1.5 years after vector administration. Mol. Ther. 18, 643–650.

Snodderly, D. M., Auran, J. D., and Delori, F. C. (1984a). The macular pigment. II. Spatial distribution in primate retinas. Invest Ophthalmol. Vis. Sci. 25, 674–685.

Snodderly, D. M., Brown, K., Delori, F. C., *et al.* (1984b). The macular pigment. I. Absorbance spectra, localization, and discrimination from other yellow pigments in primate retinas. Invest Ophthalmol. Vis. Sci. 25, 660–673.

Song, S., Scott-Jorgensen, M., Wang, J., *et al.* (2002). Intramuscular administration of recombinant adeno-associated virus 2 alpha-1 antitrypsin (rAAV-SERPINA1) vectors in a nonhuman primate model: safety and immunologic aspects. Mol. Ther. 6, 329–335.

Stieger, K., *et al.* (2008). Subretinal delivery of recombinant AAV serotype 8 vector in dogs results in gene transfer to neurons in the brain. Mol. Ther. 16, 916–923.

Stieger, K., and Lorenz, B., (2010). Gene therapy for vision loss—recent developments. Discov. Med. 10, 425–433.

Sun, X., *et al.* (2010). Gene therapy with a promoter targeting both rods and cones rescues retinal degeneration caused by AIPL1 mutations. Gene Ther. 17, 117–131.

Sundaram, V., Moore, A. T., Ali, R. R., *et al.* (2012). Retinal dystrophies and gene therapy. Eur. J. Pediatr. 171, 757–765.

Tan, M. H., *et al.* (2009). Gene therapy for retinitis pigmentosa and Leber congenital amaurosis caused by defects in AIPL1: effective rescue of mouse models of partial and complete Aipl1 deficiency using AAV2/2 and AAV2/8 vectors. Hum. Mol. Genet. 18, 2099–2114.

Timmers, A. M., Zhang, H., Squitieri, A., *et al.* (2001). Subretinal injections in rodent eyes: effects on electrophysiology and histology of rat retina. Mol. Vis. 7, 131–137.

Vandenberghe, L. H., and Auricchio, A. (2012). Novel adeno-associated viral vectors for retinal gene therapy. Gene Ther. 19, 162–168.

Vandenberghe, L. H., Bell, P., Maguire, A. M., *et al.* (2011). Cone and rod transduction with alternative AAV serotypes in the macula of nonhuman primates. Conference Proceedings. The Association for Research in Vision and Ophthalmology, Ft. Lauderdale, FL.

Wang, Y., Macke, J., Merbs, S. L., *et al.* (1992). A locus control region adjacent to the human red and green visual pigment genes. Neuron 9, 429–440.

Weiss, E. R., Ducceschi, M. H., Horner, T. J., *et al.* (2001). Species-specific differences in expression of G-protein-coupled receptor kinase (GRK) 7 and GRK1 in mammalian cone photoreceptor cells: implications for cone cell phototransduction. J. Neurosci. 21, 9175–9184.

Yang, G. S., Schmidt, M., Yan, Z., *et al.* (2002). Virus-mediated transduction of murine retina with adeno-associated virus: effects of viral capsid and genome size. J. Virol. 76, 7651–7660.

Yao, J., Feathers, K. L., Khanna, H., *et al.* (2011). XIAP therapy increases survival of transplanted rod precursors in a degenerating host retina. Invest Ophthalmol. Vis. Sci. 52, 1567–1572.

Yin, L., *et al.* (2011). Intravitreal injection of AAV2 transduces macaque inner retina. Invest Ophthalmol. Vis. Sci. 52, 2775–2783.

Zolotukhin, S. (2005). Production of recombinant adeno-associated virus vectors. Hum. Gene Ther. 16, 551–557.

Address correspondence to:
Dr. Shannon Boye
Department of Ophthalmology
College of Medicine
University of Florida
1600 SW Archer Road
Gainesville, FL 32610

E-mail: shannon.boye@eye.ufl.edu

Received for publication June 19, 2012;
accepted after revision July 8, 2012.

Published online: July 30, 2012.